

# Spatial Resolution of the Variable-Period X-Ray Standing-Wave Method as Applied to Model Membranes

Rosangela Itri, Ruitian Zhang, and Martin Caffrey

Department of Chemistry, The Ohio State University, Columbus, Ohio 43210 USA

**ABSTRACT** A series of model membranes as Langmuir-Blodgett (LB) films composed of long-chain zinc alkanooates (saturated fatty acid salts) was used to evaluate the spatial resolution of the variable-period x-ray standing-wave (XSW) technique. The chain length dependence of the zinc mean position ( $\langle z \rangle$ ) above the supporting substrate demonstrates that it is possible to detect differences in ( $\langle z \rangle$ ) of 1–2 Å. Thus 1–2 Å is the spatial resolution of the method in the current application. The data show that the chain tilt angle is chain length dependent, varying from 40° to 0° for alkanooates 18 and 24 carbon atoms long, respectively. The spread about the mean position of the zinc in the film,  $\sigma_{in}$ , was found to be independent of chain length at 10.0 Å for all members of the series.  $\sigma_{in}$  was shown to be insensitive to the presence of a “spacer”  $\omega$ -tricosenoic acid ( $\omega$ TA) bilayer placed between the zinc alkanooate LB film and the coated gold mirror. However, an overlayer of  $\omega$ TA sharpened the zinc ion distribution and lowered the chain tilt angle. This study provides important information regarding sample composition and constitution that facilitates membrane structure determination by XSWs.

## INTRODUCTION

The variable-period x-ray standing wave (XSW) method has been used as a probe of the structure and element distribution in model membrane systems such as Langmuir-Blodgett (LB) and self-assembled lipid/protein films (Bedzyk et al., 1990; Wang et al., 1991, 1992, 1994a,b). The method is based on the total external or specular reflection of an x-ray plane wave from a mirror surface (Bedzyk et al., 1989). Standing waves are established above the mirror surface in the region where the incident and reflected beams overlap. In the course of a so-called  $\theta$ -scan, where the angle between the sample and the incident beam  $\theta$  is changed, the XSW nodes and antinodes pass through a probe or marker atom-containing adlayer, giving rise to minima and maxima, respectively, in the corresponding x-ray fluorescence yield profile (Bedzyk et al., 1989). An analysis of the fluorescence yield profile provides information about the mean position (referred to as the first moment,  $\langle z \rangle$ , where the  $z$  direction is normal to the mirror surface) and variance (referred to as the second moment,  $\sigma^2$ , where  $\sigma$  is the distribution half-width) of the probe atom distribution in the adsorbed layer.

Ultimately, we wish to use the XSW method to investigate macromolecule-membrane interactions. For example, the difference in  $\langle z \rangle$  value of two marker atoms at known sites in a membrane-bound protein can provide information

about the orientation of the protein in or on the membrane (Caffrey and Wang, 1995). As a first step toward realizing such goals, it is necessary to establish the spatial resolution of the XSW technique. We have addressed this issue in the current work by evaluating the minimum distance between two probe atom positions in separate films that can be determined by using variable-period XSWs. Henceforth in this study, the latter will serve as a working definition for “spatial resolution” as applied to the XSW method. Accordingly, XSW measurements have been made on a series of LB films deposited on gold mirrors rendered hydrophobic with a self-assembled octadecanethiol (ODT) monolayer. These films are composed of inverted bilayers of zinc alkanooates with chain lengths ranging from C16 to C24, where C represents the number of carbon atoms in the fatty acid. The expectation is that the zinc layer would differ in  $\langle z \rangle$  from its nearest neighbor in the series by a maximum of 1.27 Å, corresponding to a single methylene ( $-\text{CH}_2-$ ) increment measured along the chain axis. In the course of making these measurements, we observed different increment values between members of the homologous alkanooate series, indicating distinct orientations of the hydrocarbon chain axes in relation to the gold mirror surface normal. Included in this study is a demonstration that the distance between the marker zinc layer and the adjacent air/lipid interface can influence  $\langle z \rangle$  and  $\sigma$  of the zinc atoms within the LB film. In addition, we have measured the intrinsic marker atom distribution,  $\sigma_{in}$ , by deconvoluting mirror surface roughness,  $\sigma_r$ , obtained from reflectivity data, from  $\sigma$ .  $\sigma_{in}$  is shown to be sensitive to the composition of the lipid film.

Received for publication 21 January 1997 and in final form 23 May 1997.

Address reprint requests to Dr. Martin Caffrey, Department of Chemistry, The Ohio State University, 120 W. 18th Ave., Columbus, OH 43210. Tel.: 614-292-8437; Fax: 614-292-1532; E-mail: caffrey@chemistry.ohio-state.edu.

Dr. Itri's permanent address is Instituto de Física da Universidade de São Paulo, C.P. 66318, São Paulo, SP, 05389-970, Brazil.

Dr. Zhang's present address is Chemistry Division, Argonne National Laboratory, 9700 S. Cass Ave, Argonne, IL 60439.

© 1997 by the Biophysical Society

0006-3495/97/09/1506/10 \$2.00

## THEORY

The following summarizes the essentials of the theory pertaining to XSW analysis. The fluorescence yield profile,  $Y(q)$ , recorded in a typical XSW measurement and corre-

sponding to an arbitrary probe atom distribution,  $\rho(z)$ , can be written as

$$Y(q) = \int \rho(z)I(q, z) dz \quad (1)$$

where  $I(q, z)$  is the XSW electric field intensity generated in the adlayer above the mirror surface,  $q (= 4\pi \sin \theta/\lambda)$  is the momentum transfer in the mirror normal direction, and  $\lambda$  is the x-ray wavelength.

A Gaussian distribution function is generally used to describe  $\rho(z)$  as (Bedzyk et al., 1989, 1990; Wang et al., 1991, 1992, 1994a,b; Kirchner et al., 1995)

$$\rho(z) = \exp(- (z - \mu_g)^2/2\sigma_g^2) \quad (2)$$

where  $\mu_g$  is the position along the  $z$  direction of maximum probability in the distribution and  $\sigma_g$  is the Gaussian standard deviation. It is noted that the first moment,  $\langle z \rangle$ , and second moment,  $\sigma^2$ , of the distribution are related to  $\mu_g$  and  $\sigma_g$ , respectively, through

$$\langle z \rangle = \mu_g + \sigma_g^2/N[\exp(-\mu_g^2/2\sigma_g^2) - \exp(-(d_L - \mu_g)^2/2\sigma_g^2)] \quad (3)$$

and

$$\sigma^2 = K - (\langle z \rangle - \mu_g)^2 \quad (4)$$

where  $N$ , a normalization factor, takes the form

$$N = \sigma_g(\pi/2)^{1/2}[\text{erf}(\mu_g/2^{1/2}\sigma_g) + \text{erf}((d_L - \mu_g)/2^{1/2}\sigma_g)] \quad (5)$$

In Eqs. 5 and 4, respectively,  $\text{erf}(x)$  is the error function and  $K$  is

$$K = \sigma_g^2(1 - [\mu_g \exp(-\mu_g^2/2\sigma_g^2) + (d_L - \mu_g) \cdot \exp(-(d_L - \mu_g)^2/2\sigma_g^2)]/N) \quad (6)$$

For a Gaussian distribution centered far from the lipid layer boundaries, such that  $(d_L - \mu_g)/\sigma_g \gg 1$  or  $\mu_g/\sigma_g \gg 1$ , we find that  $\langle z \rangle = \mu_g$  in Eq. 3 and  $\sigma = \sigma_g$  in Eq. 4. Because most of the samples used in this study have the zinc marker layer positioned relatively close to the lipid adlayer/air interface such that  $(d_L - \mu_g)/\sigma_g \ll 1$ , the Gaussian distribution is truncated at  $z = d_L$ . As a consequence,  $\mu_g \neq \langle z \rangle$  and  $\sigma_g \neq \sigma$ . For this reason, the results presented below are described in terms of  $\langle z \rangle$  (Eq. 3) and  $\sigma$  (Eq. 4) of the corresponding truncated Gaussian zinc distribution.

## MATERIALS AND METHODS

### Sample preparation

Octadecanethiol (ODT) (98% purity) was purchased from Aldrich (Milwaukee, WI);  $\omega$ -tricosenoic acid (22-tricosenoic acid) was obtained from Eastman Kodak Co. (Rochester, NY); and fatty acids, with chain lengths ranging from C16 to C24, were from Nu-Chek-Prep (Elyson, MN). All were used without further purification.  $\text{ZnCl}_2$  (99.1%) was obtained from Baker (Phyllipsburg, NJ), and both  $\text{NaHCO}_3$  (99.9%) and tetrahydrofuran

(99.9%) were supplied by Mallinckrodt (Paris, KY). Chloroform was purchased from Sigma (St. Louis, MO). Water, purified by using a Milli-Q Reagent water system (Millipore Corp., Bedford, MA), consisting of a carbon filter cartridge, two ion-exchange filter cartridges, and an organic removal cartridge, with a specific resistance of 18 M $\Omega$  cm, was used throughout.

Mirrors (50 mm  $\times$  12 mm) were obtained commercially (Guernsey Coating Laboratories, Ventura, CA) and consisted of 1000 Å of gold thermoevaporated onto a chromium (250-Å layer thickness)-coated silicon substrate (0.5 mm thick). Mirrors were rinsed in a ultrasonic bath of chloroform for 3 min and plasma cleaned (model PDC-3XG; Harrick Scientific Corp., Ossining, NY; argon pressure < 1.0 torr; high power setting) for 10 min to expose a fresh gold surface before being coated with organic films. Immediately upon removal from the plasma cleaner, the mirror was immersed in a 1 mM solution of ODT in tetrahydrofuran freshly distilled over potassium and incubated at room temperature (18°C) for at least 12 h. The mirrors were subsequently rinsed with freshly distilled tetrahydrofuran to remove excess ODT. The thickness of the self-assembled ODT monolayer was measured by ellipsometry (model L116C; Gaertner Scientific Corp., Chicago, IL).

Three sample types (A, B, and C) were included in this study. Their constitution is shown schematically in Fig. 1. Sample series A consisted of an inverted bilayer of zinc alkanoate (C16–C24) on an ODT-coated gold mirror and is denoted  $\text{Au/ODT}_m/\text{ZnA}_{ib}$ , where the subscripts  $m$  and  $ib$  represent monolayer and inverted bilayer, respectively. Sample B has the following constitution:  $\text{Au/ODT}_m/\text{ZnA}_{ib}/\omega\text{TA}_{ib}$ , where  $\text{ZnA}$  represents C20 and  $\omega\text{TA}_{ib}$  represents an upper inverted bilayer of  $\omega\text{TA}$ . Sample series C corresponds to  $\text{Au/ODT}_m/2\omega\text{TA}_{ib}/\text{ZnA}_{ib}$ , where  $\text{ZnA}$  represents C21 and C24.

The deposition of zinc alkanoate LB films on ODT-coated mirrors was performed using a KSV MiniTrough system (KSV Instruments, Riverside, CT) with a trough surface area of 35.5 cm  $\times$  7.5 cm in a clean room at 18°C as follows. A 1 mg/ml solution of each alkanoic acid in chloroform was placed dropwise, by means of a 100- $\mu\text{l}$  Hamilton syringe, on an aqueous subphase containing 0.1 mM  $\text{ZnCl}_2$  and 0.1 mM  $\text{NaHCO}_3$ , pH =  $7.0 \pm 0.2$ , measured with a pH meter (model 910; Fisher Scientific, Pittsburgh, PA) until an increase in the surface pressure,  $\pi$ , from 0 to 1–3 mN/m was observed. The film was allowed to sit at  $\pi = 1$ –3 mN/m for 20 min, was subsequently compressed to 30 mN/m with a barrier speed of 1–2 mm/min, and was then incubated for an additional 20 min at this new pressure. The compressed film was transferred to the gold mirror at a deposition rate (vertical translation of mirror) of 3 mm/min and  $\pi = 30$  mN/m. At this pressure, all films are in the solid phase, which lies between the liquid-solid phase transition and the collapse pressure as observed from the corresponding  $\pi$ -surface area isotherms (data not shown). Samples so prepared correspond to sample series A.

Sample B was prepared as follows. A mirror, initially covered with ODT and one inverted bilayer of zinc arachidate (C20), was coated with an inverted bilayer of  $\omega\text{TA}$ . For this purpose, a 1 mg/ml solution of  $\omega\text{TA}$  in chloroform was spread on a Milli-Q water subphase, as described above. The solvent was allowed to evaporate for at least 10 min before the film was compressed to 30 mN/m at a barrier speed of 3 mm/min. The compressed film was incubated for 20 min at 30 mN/m and was then deposited at a rate of 3 mm/min at this same surface pressure.

Series C samples, incorporating two inverted bilayers of  $\omega\text{TA}$  as a spacer layer between the ODT-coated mirror surface and the inverted bilayer of zinc alkanoate, were prepared with zinc heneicosanoate (C21) and zinc lignocerate (C24). Conditions used were identical to those for sample series A and sample B above, with the obvious differences in the order of adlayer deposition.

In the course of LB film deposition, monolayer transfer ratios were measured by monitoring the decrease in film area at the air/subphase interface per unit of substrate surface area passing through the interface. A transfer ratio of unity ( $\pm 10\%$ ) was observed for all of the samples, with the exception of heptadecanoic acid (C17) in sample series A. This fatty acid gave an unrealistic transfer ratio of  $\sim 2$  with an aberrant total sample thickness (measured by ellipsometry) and, as a result, was eliminated from the study. Ellipsometry was used to measure the thickness of successive

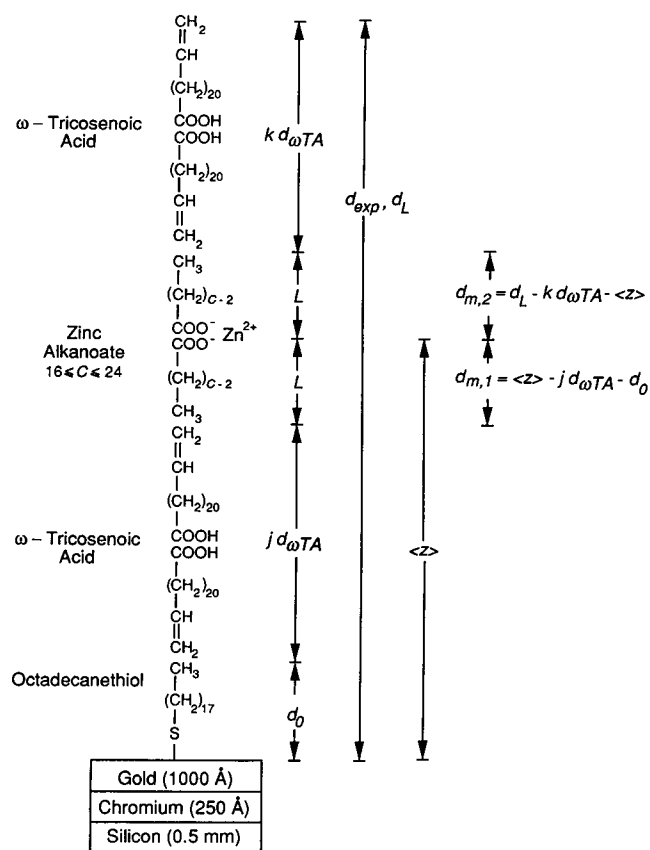


FIGURE 1 Schematic of the gold mirror and deposited films. Gold was thermoevaporated as a 1000-Å-thick film on a piece of chromium-coated silicon. Before depositing the LB layers of  $\omega$ TA and zinc alkanolate, the plasma-cleaned gold surface was rendered hydrophobic with a self-assembled ODT monolayer. For sample series A (Au/ODT<sub>m</sub>/ZnA<sub>ib</sub>):  $j = k = 0$ ; sample B (Au/ODT<sub>m</sub>/ZnA<sub>ib</sub>/ωTA<sub>ib</sub>):  $j = 0, k = 1$ ; sample series C (Au/ODT<sub>m</sub>/2 ωTA<sub>ib</sub>/ZnA<sub>ib</sub>):  $j = 2, k = 0$ . The distance parameter,  $d_0$ , was determined by ellipsometry, and  $d_{\omega TA}$  and  $L$  were calculated from the corresponding molecular structures based on the following assumptions and bond angles and lengths. Hydrocarbon chains were assumed to be in the all-*trans*, fully extended conformation with C-C, C=C, C-H, C-O, C-S, O-H, and S-Au bond lengths of 1.53 Å, 1.34 Å, 1.10 Å, 1.43 Å, 1.82 Å, 0.97 Å, and 1.34 Å, respectively (Gordon and Ford, 1972). For O-Zn, a bond length of 2.05 Å was used (Carrell et al., 1988). The bond angles used for C-C-C, C=C-C, C=C-H, C-CO-O, CO-O-H, CO-O-Zn, and C-S-Au were 112°, 122°, 119°, 120°, 120°, 120°, and 105° (Gordon and Ford, 1972; Carrell et al., 1988). Accordingly, the long-axis dimension is 25.02 Å for ODT and 30.95 Å for ωTA ( $d_{\omega TA} = 61.90$  Å) and equals  $L = [3.90 + (C - 1) 1.27]$  Å for the zinc alkanolates, where  $C$  is the total number of carbon atoms in the chain.  $d_{exp}$  is given as a sum of  $d_0 + 2L + (j + k)d_{\omega TA} \cdot \langle z \rangle$  and  $d_L$  were obtained from fluorescence yield data.  $d_{m,1}$  and  $d_{m,2}$  correspond to the thicknesses of the first and second zinc alkanolate monolayers and are calculated as indicated in the figure.

layers immediately after each deposition segment was completed. The corresponding film thicknesses were used to evaluate deposition quality by comparing them with the expected total thickness,  $d_{exp}$ , of the lipid adlayer (Fig. 1 and Table 1).  $d_{exp}$  was calculated as the sum of the thickness of an ODT monolayer,  $d_0$ , plus twice that of a zinc alkanolate monolayer,  $L$ , in the case of sample series A. Details of how  $L$  is calculated are given in Fig. 1. For samples containing ωTA (sample B and sample series C),  $d_{exp}$  includes the thickness of an inverted bilayer of ωTA estimated at 61.90 Å (Fig. 1).

TABLE 1 Self-assembled monolayer and Langmuir-Blodgett film thickness (in ångströms) measured by ellipsometry and calculated from molecular structure

Sample series*	Chain length	Ellipsometry <sup>#</sup>				Calculated <sup>§</sup>	
		ODT	2 ωTA <sub>ib</sub>	ZnA <sub>ib</sub>	ωTA <sub>ib</sub>	$L$	$d_{exp}$
A	C16	22 ± 1		64 ± 1		22.95	68.10
	C18	22 ± 1		69 ± 1		25.49	73.18
	C19	22 ± 1		74 ± 1		26.76	75.72
	C20	22 ± 2		79 ± 1		28.03	78.26
	C21	22 ± 2		80 ± 1		29.30	80.80
	C22	22 ± 1		82 ± 2		30.57	83.34
	C23	22 ± 2		90 ± 1		31.84	85.88
	C24	22 ± 2		94 ± 1		33.11	88.42
B	C20	22 ± 2		78 ± 1	147 ± 3	28.03	140.16
C	C21	23 ± 1	160 ± 1	220 ± 1		29.30	204.60
	C24	23 ± 1	160 ± 4	234 ± 4		33.11	212.22

\*See legend, Fig. 1.

<sup>#</sup>Thickness is reported as the average of measurements (six total) performed on three distinct parts of duplicate mirrors. The errors were calculated as half of the interval between the maximum and minimum values.

<sup>§</sup> $L$  corresponds to the calculated thickness of the zinc alkanolate monolayer, and  $d_{exp}$  represents the expected total adlayer thickness (see text and Fig. 1 for details), with an average ODT thickness  $d_0 = 22.2 \pm 0.5$  Å (this table) and an ωTA thickness  $d_{\omega TA} = 61.90$  Å.

## X-ray standing-wave measurements

The XSW measurements were carried out on the X15A beam line of the National Synchrotron Light Source (NSLS), Brookhaven National Lab, at 2.6 GeV and 140–280 mA of total electron beam current. Polychromatic x-rays from the storage ring were monochromatized to 9.8 keV with a pair of flat germanium (111) crystals (2.0 cm wide × 2.5 cm long) to optimally excite zinc K<sub>α</sub> fluorescence. The monochromated beam was then collimated to 40 μm in height and 2 mm in width by X-Y slits (model 3013; Huber, Rimsting, Germany). Collimated beam intensity was monitored continuously by a 2.5-cm-long, air-filled ionization chamber. The relevant distances along the x-ray flight path, which includes the synchrotron source, monochromators, slit, and sample, were 17 m, 40 cm, and 18 cm, respectively.

X-ray fluorescence from the sample was recorded by using an energy-dispersive solid-state Si(Li) detector (model LS83180; Princeton Gamma-Tech, Princeton, NJ) with an active input area of 80 mm<sup>2</sup> and an energy resolution of 180 eV. A typical fluorescence spectrum is shown in Fig. 2. The snout of the detector was positioned perpendicular to and in the same horizontal plane as the incident beam to reduce the contribution from scattered x-rays. The distance between the entrance window of the Si(Li) detector and the center of the footprint was 32 mm. Signal pulses from the detector were then amplified by a spectroscopy amplifier (model TC244; Tennelec, Oak Ridge, TN). Detector dead time correction was implemented by using a pulser from a random pulse generator (model DB-2; Berkeley Neclonics Corp., Berkeley, CA) positioned close (in energy) to the fluorescence signal of interest and with a similar count rate. The entire fluorescence spectrum from 0 to 12.5 keV (512 channels) was recorded at each incident angle. Sample reflectivity was recorded simultaneously with the fluorescence measurement by means of a pin-diode detector (UV-44BQ; Egg-Ortec, Oak Ridge, TN).

The sample was placed on a home-built aluminum holder attached to a goniometer head (model 1003; Huber). The 1003 head was used to adjust the vertical height and tilt angle,  $\zeta$ , of the sample.  $\zeta$  is defined as a rotation about an axis passing along the mirror surface in the direction and at the center of the incident x-ray beam that runs parallel to the mirror surface (zero incident angle). The 1003 head was in turn mounted on a Huber 410 goniometer, which was used to control the angle of incidence,  $\theta$ , between the x-ray beam and the sample. The  $\theta$  axis of rotation is perpendicular to the incident x-ray beam and lies in the plane of the synchrotron electron

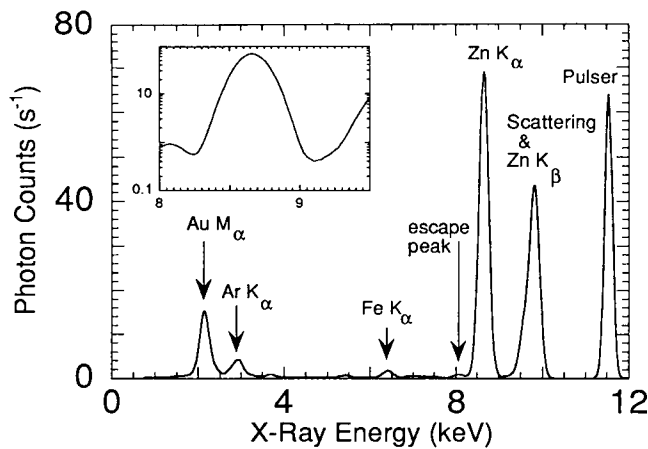


FIGURE 2 X-ray fluorescence spectrum from a series A sample composed of an inverted bilayer of zinc heneicosanoate (C21) recorded at an incident beam energy of 9.8 keV summed in the incident angle range from 0 to 12 mrad. Details of the experimental set-up are described under Materials and Methods. The zinc  $K_{\alpha}$  fluorescence peak at 8.64 keV is well resolved from the detector escape peak at 8.06 keV. An expanded view of the zinc  $K_{\alpha}$  peak, in the form of a semilog plot, is shown in the inset. Gold  $M_{\alpha}$  (2.12 keV), argon  $K_{\alpha}$  (2.96 keV), and iron  $K_{\alpha}$  (6.40 keV) fluorescence lines are present in the spectrum.

orbit. Sample alignment began by orienting the mirror surface to an approximately horizontal position. The vertical position of the mirror was adjusted until the incident beam intensity was cut in half, as judged by the image of the x-ray beam on an image intensifier (P/N 510-3603-300; Varo, Garland, TX) placed downstream of the sample.  $\theta$  was slowly increased to reveal a reflected beam, and  $\zeta$  was adjusted until the long axis of the direct and reflected beams, as viewed on the image intensifier, were parallel. This defined  $\zeta = 0$ , which was where all subsequent XSW and reflectivity measurements were made. At this point, the image intensifier was replaced by a pin diode detector. To calibrate the  $\theta$ -scale, a reflectivity profile from 0 to 12 mrad, was recorded in 0.5-mrad steps with a counting time of 1 s/step. The value of  $\theta$  where the reflected intensity was half that of the totally reflected beam was defined operationally as the gold critical angle,  $\theta_{c,\text{gold}}$ , for purposes of data collection. A more accurate determination of  $\theta_{c,\text{gold}}$  was made during data analysis as described below. Once the  $\theta$ -scale was so defined,  $\theta$  was reset to zero and the height of the sample was adjusted once again to cut the incident beam intensity in half.

With the above experimental arrangement in place, a counting time of 30 s at each value of  $\theta$  provided zinc fluorescence data from a typical zinc alkanolate LB film with 1% counting statistics at the peak of the fluorescence yield profile. Thus a  $\theta$  scan consisting of 60 angular steps from 0 to 12 mrad required 30 min to complete. All measurements were made at 27°C, the temperature measured inside the X15A hutch.

### XSW data analysis

An accurate measure of total fluorescence counts at each incident angle  $\theta$  was made by determining the integrated area beneath the zinc  $K_{\alpha}$  peak centered at 8.64 keV. A background, defined by drawing a straight line through the intensity minima at 8.5 and 9.2 keV (see inset in Fig. 2), was subtracted from the total integrated counts in this energy range. The fluorescence intensity was normalized to the changing count rate of the direct beam and corrected for detector dead time and detector solid angle, as described previously (Wang et al., 1994a).

The values of the refractive index decrement,  $\delta$ , and the absorption index,  $\beta$ , used in calculating the x-ray reflectivity at an incident x-ray photon energy of 9.8 keV were as follows:  $\delta = 2.99 \times 10^{-5}$ ,  $\beta = 2.20 \times 10^{-6}$  for gold (evaluated from recent reflectivity measurements showing

that these values are 3% smaller than those for bulk gold) (Dr. Jin Wang, Argonne National Lab, personal communication);  $\delta = 2.5 \times 10^{-6}$ ,  $\beta = 2.24 \times 10^{-9}$  for lipid (Wang et al., 1994a); and  $\delta = 3.80 \times 10^{-6}$ ,  $\beta = 4.00 \times 10^{-7}$  for the silicon substrate. It was noticed that the effect on reflectivity of the thin chromium layer between the gold and the silicon is negligible and hence is not considered here. At 9.8 keV, the critical angle,  $\theta_c (= (2\delta)^{1/2})$ , of the gold mirror, of the lipid layer and of the silicon, in vacuo, is 7.73 mrad, 2.24 mrad, and 2.76 mrad, respectively. The period of the XSW at  $\theta_c$  is referred to as the critical period,  $D_c (= \lambda/2 \sin \theta_c)$ , and equals 82 Å for gold.

The effect of gold mirror surface roughness on the x-ray reflectivity was taken into account through the Nevot-Croce factor (Sinha et al., 1988; de Boer, 1994, 1995, 1996).

A  $\chi^2$  minimization procedure was used in fitting both the reflectivity and the fluorescence data to the corresponding theoretical profiles. Data were fitted in the angular range from 3 to 9 mrad. Data for  $\theta < 3$  mrad were not used in the analysis, primarily because of poor penetration into the lipid adlayer below its  $\theta_c$ . Data for  $\theta > 9$  mrad were not included in the analysis either, because reflectivity and fluorescence intensities are weak and were not recorded with high accuracy in this angular range.

Three adjustable parameters were used to fit the reflectivity data. They include an angular shift,  $\Delta\theta$ , used to set  $\theta$  on an absolute scale, the gold mirror surface roughness,  $\sigma_r$ , and the total thickness of the lipid adlayer,  $d_L$ .  $\Delta\theta$  is determined by matching the experimental and theoretical reflectivity profiles in the vicinity of  $\theta_{c,\text{gold}}$ , where reflectivity intensity changes dramatically (see Fig. 3). In the course of this study, we have found that  $\Delta\theta$

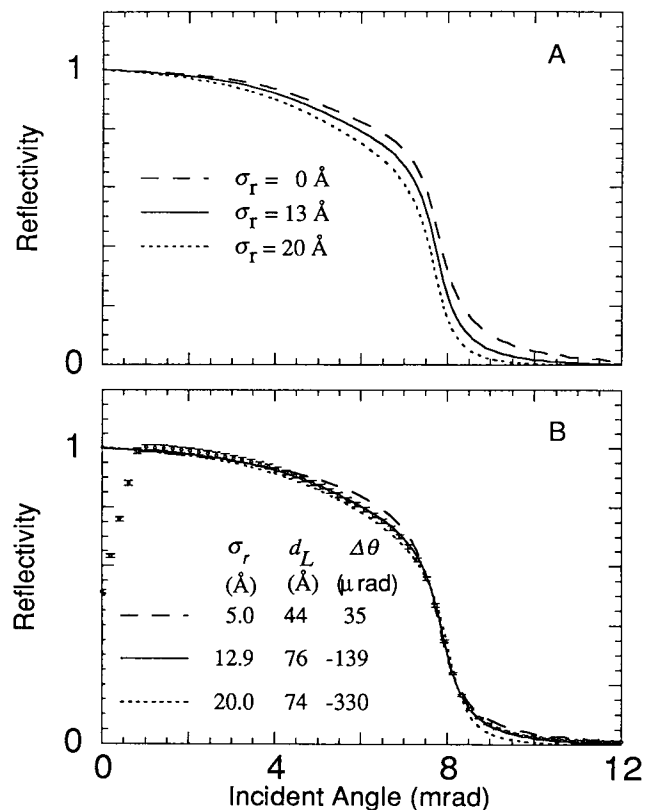


FIGURE 3 (A) Reflectivity profile calculated for mirrors with a surface roughness value  $\sigma_r = 0$  Å (---), 13 Å (—), and 20 Å (····) and a total lipid film thickness  $d_L = 80$  Å. (B) Experimental (circles) and theoretical (lines) angular dependence of the specular reflectivity for a series A sample (C19). Theoretical reflectivity profiles were calculated using the indicated parameters for gold mirror roughness,  $\sigma_r$ , total adlayer thickness,  $d_L$ , and angular shift correction,  $\Delta\theta$ . The solid line corresponds to the best fit as determined by  $\chi^2$  minimization.

and  $\sigma_r$  are coupled parameters as explained below. Roughness gives rise to diffuse scattering and reduces the reflectivity intensity at all values of  $\theta$ . Fig. 3 A illustrates this effect for a sample with  $d_L = 80 \text{ \AA}$  and values of  $\sigma_r = 0, 13, \text{ and } 20 \text{ \AA}$ . Clearly, roughness causes a shift in the reflectivity profile to lower  $\theta$ -values, not unlike the effect of  $\Delta\theta$ . Consequently, a larger roughness value could possibly be accounted for by a negative  $\Delta\theta$ .

To overcome this parameter coupling problem, the reflectivity fit was repeated several times using a  $d_L$  value, obtained by ellipsometry, as an input fitting parameter and different initial values of  $\Delta\theta$  and  $\sigma_r$ . Fig. 3 B shows an example of this approach as applied to C19 in sample series A (open circles), for three different sets of starting parameters. The corresponding best fitting values are  $d_L = 76 \text{ \AA}$ ,  $\Delta\theta = -0.139 \text{ mrad}$ , and  $\sigma_r = 12.9 \text{ \AA}$  (solid line, set A);  $d_L = 74 \text{ \AA}$ ,  $\Delta\theta = -0.330 \text{ mrad}$ , and  $\sigma_r = 20.0 \text{ \AA}$  (dotted line, set B); and  $d_L = 44 \text{ \AA}$ ,  $\Delta\theta = -0.035 \text{ mrad}$ , and  $\sigma_r = 5.0 \text{ \AA}$  (dashed line, set C), for which  $\chi^2 = 0.6, 10, \text{ and } 19$ , respectively. An excellent fit was obtained for parameter set A, and the corresponding  $d_L$  value of  $76 \text{ \AA}$  matches the expected value,  $d_{exp}$ , of  $75.72 \text{ \AA}$  (Table 1). Parameter set B also includes a reasonable  $d_L$  value of  $74 \text{ \AA}$ . However, the quality of the fit ( $\chi^2 = 10$ ) is significantly poorer than for set A, with a significant mismatch between experiment and theory both above and below  $\theta_{c,gold}$ . Set C clearly underestimates both  $d_L$  and  $\sigma_r$ , and the corresponding  $\chi^2$  value is high. In this situation, parameter set A best described the data, as evidenced by the smallest residual  $\chi^2$  value and the physically realistic parameters.

In the course of this study, the best set of  $d_L$ ,  $\Delta\theta$ ,  $\sigma_r$  parameters was selected using the minimum  $\chi^2$  values from the fit constrained to physically reasonable values for  $d_L$  and  $\sigma_r$ . The surface roughness value so determined was used in subsequent XSW  $E$ -field intensity and fluorescence calculations. The angular shift  $\Delta\theta$ , which ranged from  $-0.3$  to  $0.3 \text{ mrad}$ , was used to correct the  $\theta$  scale of the corresponding fluorescence profile data.

The fluorescence yield profiles were fitted according to Eq. 1, assuming a Gaussian distribution (Eq. 2) of zinc ions, with the value of  $z$  ranging from 0 to  $d_L$ . The three adjustable parameters used to fit the fluorescence data include  $d_L$ ,  $\mu_g$ , and  $\sigma_g$ . The results are presented in terms of  $\langle z \rangle$  (Eq. 3) and  $\sigma$  (Eq. 4) of the corresponding truncated Gaussian distribution, as explained above under Theory. It will be shown separately that the fluorescence yield profile is more sensitive to the overall organic film thickness,  $d_L$ , than is the corresponding reflectivity profile (manuscript in preparation). Accordingly,  $d_L$  values extracted from fluorescence yield data were used in the analysis presented below.

To summarize this section, we reiterate that 1)  $\langle z \rangle$ ,  $\sigma$ , and  $d_L$  were obtained from an analysis of the fluorescence yield data; 2) ellipsometry was used to measure directly SAM and LB film thicknesses; and 3) the values of  $d_{\omega TA}$ ,  $d_{m,1}$ ,  $d_{m,2}$ ,  $d_{exp}$ , and  $L$  were calculated as described in the legend to Fig. 1.

## RESULTS

Table 1 summarizes the self-assembled ODT monolayer thickness measured by ellipsometry for the 22 samples included in this study. The average thickness,  $d_0$ , is  $22.2 \pm 0.5 \text{ \AA}$ . The length of an ODT molecule, measured along its long axis and assuming a fully extended, all-*trans* configuration, is  $25 \text{ \AA}$  (see Fig. 1). Thus a  $d_0$  value of  $22.2 \text{ \AA}$  suggests that the octadecyl chains are tilted at an angle of  $\sim 27.5^\circ$  from the normal to the mirror surface. The latter agrees with infrared spectroscopy results (Porter et al., 1987), which show tilt angles from  $20^\circ$  to  $30^\circ$  for monolayers of alkyl thiolates with chain lengths ranging from C16 to C22 deposited on gold substrates.

Table 1 also includes data for ellipsometry thickness measurements performed during the course of sample preparation, along with the expected values for total adlayer thickness,  $d_{exp}$ , based on known molecular structures. Over

a 2-month period, we found that the total adlayer thickness measured by ellipsometry remained constant within the uncertainties of the measurements, as shown in Table 1.

In what follows, we describe the results of reflectivity and XSW measurements performed on a series of zinc alkanolate-containing LB films. The aim of these measurements was to establish the spatial resolution of the variable-period XSW technique (realized with sample series A), and to evaluate how film constitution affects the structural integrity of the lipid adlayer (sample B, series C).

### Series A (Au/ODT<sub>m</sub>/ZnA<sub>1b</sub>)

Fig. 4 shows the experimental and theoretical reflectivity and fluorescence profiles for all zinc-containing samples in this series. The values of the interface roughness,  $\sigma_r$ , total lipid thickness,  $d_L$ , mean position,  $\langle z \rangle$ , and half-width,  $\sigma$ , of the zinc distribution obtained by  $\chi^2$  fitting to these data are presented in Table 2. The agreement between the experimental and the theoretical reflectivity curves is remarkably good. From these data, a  $\sigma_r$  value of  $12.9 \pm 0.3 \text{ \AA}$  was obtained when averaged over all series A samples (Table 2). The latter was subsequently used in fitting the experimental fluorescence yield profiles.

The agreement between the experimental and theoretical fluorescence yield profiles is also good for the entire set of samples in series A with the exception of C16, the shortest zinc alkanolate in the series (Fig. 4 I). In this case, the fluorescence yield profile could not be described with any reasonable model for zinc distribution, including one in which the zinc is distributed uniformly in the lipid adlayer (solid line in Fig. 4 I). As a result, this sample was excluded from further consideration. From the fluorescence data we determined the  $\langle z \rangle$  and  $\sigma$  of the zinc distribution in the film (Table 2). The data demonstrate clearly that  $\langle z \rangle$  is sensitive to alkanolate chain length. From this dependence, we will determine the spatial resolution of the XSW method, as discussed below. Interestingly, the  $\sigma$  of the zinc distribution,  $16.3 \pm 0.2 \text{ \AA}$ , is insensitive to alkanolate chain length (Table 2).

### Sample B (Au/ODT<sub>m</sub>/ZnA<sub>1b</sub>/ $\omega$ TA<sub>1b</sub>)

This sample was investigated with a view to determining the effect of a lipid overlayer and a larger distance separating the zinc-containing adlayer and the air/lipid interface on  $\langle z \rangle$  and  $\sigma$  of the zinc distribution. The corresponding reflectivity and fluorescence data are shown in Fig. 5. The fit parameters,  $\sigma_r$ ,  $d_L$ ,  $\langle z \rangle$ , and  $\sigma$ , for this sample are included in Table 2.

Unlike the reflectivity data for series A samples, the reflectivity profile for sample B is modulated in the low-angle region (Fig. 5 A). Such modulation is due to the presence of a thicker adlayer (Tables 1 and 2) and arises from interference between reflections generated at the air/film interface and those generated at the film/mirror inter-

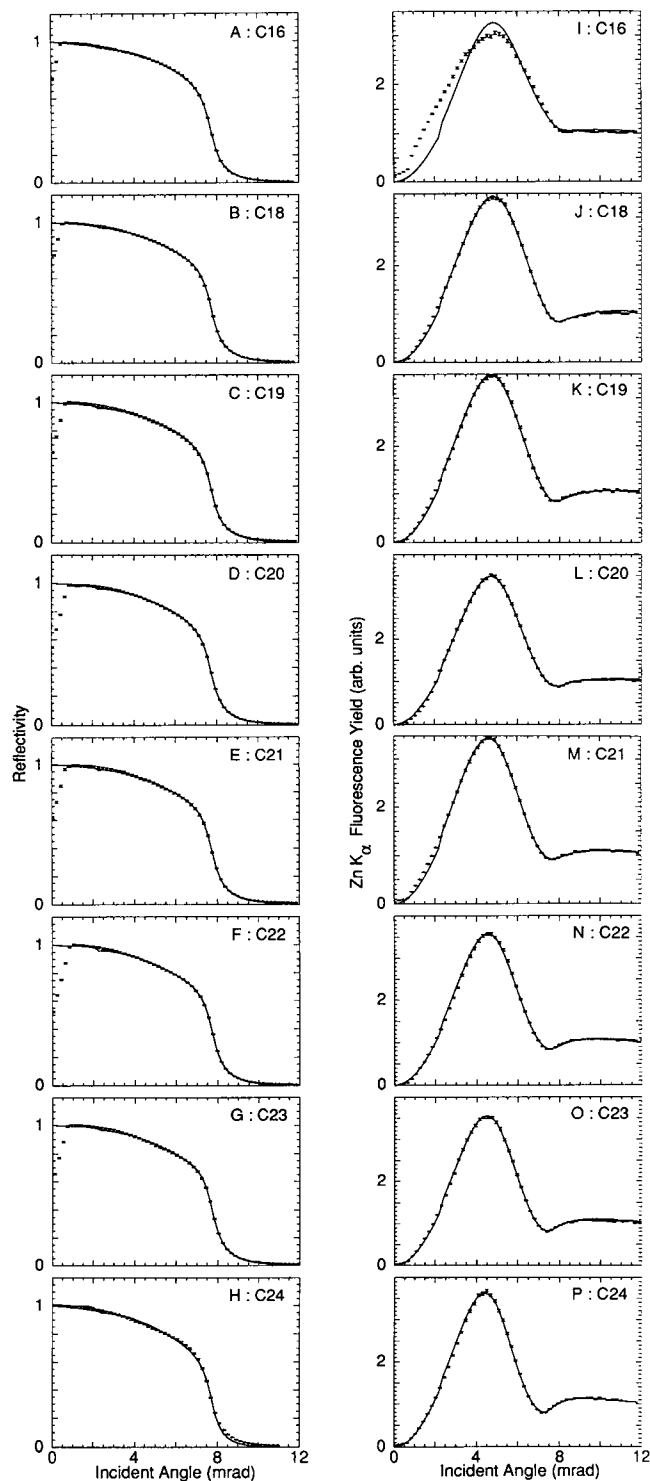


FIGURE 4 The experimental (*circles*) and theoretical (*solid lines*) angular dependence at 9.8 keV of the specular reflectivity (A–H) and zinc  $K_{\alpha}$  fluorescence yield (I–P) for samples in series A consisting of a self-assembled ODT monolayer covered by an inverted bilayer of zinc alkanolate with hydrocarbon chain lengths, as indicated in the figure.

face (Wang et al., 1991). The surface roughness value of  $12.7 \pm 0.3 \text{ \AA}$  extracted from the reflectivity data is the same as observed for series A samples above.

The fluorescence data on sample B are consistent with a average  $\langle z \rangle$  value of  $47.8 \pm 0.2 \text{ \AA}$ , and with a  $\sigma$  value of  $14.8 \pm 0.1 \text{ \AA}$ . The values obtained for the corresponding “uncoated” samples in series A are  $46.1 \pm 1.0 \text{ \AA}$  and  $16.0 \pm 1.0 \text{ \AA}$ . These data suggest that the effect of the  $\omega$ TA overlayer on the structure of the zinc alkanolate film is minimal. We do note, however, that the fluorescence profiles of the two sample types are quantitatively different, despite having very similar zinc layer positions and distributions (compare Figs. 4 L and 5 B). This demonstrates the sensitivity of the fluorescence yield profile to adlayer thickness as noted.

### Series C ( $\text{Au}/\text{ODT}_m/2 \omega\text{TA}_{ib}/\text{ZnA}_{ib}$ )

Series C was designed to evaluate the effect of including a spacer layer between the hydrophobic mirror surface and the zinc alkanolate LB film on the structure characteristics of the latter. For this purpose, two inverted bilayers of  $\omega$ TA were used as spacers upon which was positioned inverted bilayers of either zinc heneicosanoate (C21) or zinc lignocerate (C24). The reflectivity and fluorescence data, along with the best fitting parameters for the series C samples, are presented in Fig. 6 and Table 2.

The reflectivity data for both samples in this series show two modulations in the low-angle region attributable to their considerable adlayer thickness. The fluorescence yield profiles for these samples also contain modulations (Figs. 6, B and D). These are a consequence of a changing XSW period that drops from infinity at  $\theta = 0^\circ$  to  $82 \text{ \AA}$  at  $\theta_{c,\text{gold}}$  (Wang et al., 1991). The fluorescence data are consistent with average  $\langle z \rangle$  values of  $171.6 \pm 1.2 \text{ \AA}$  and  $178.0 \pm 1.7 \text{ \AA}$  and  $\sigma$  values of  $18.0 \pm 1.0 \text{ \AA}$  and  $15.8 \pm 0.5 \text{ \AA}$  for C21 and C24, respectively. These results will be discussed below.

## DISCUSSION

To facilitate a discussion of the data presented above, this section is divided into two subsections. The first addresses the spatial resolution and reproducibility of the XSW method. The second part is concerned with LB film structure and zinc distribution within the lipid adlayer.

### Spatial resolution and reproducibility of the XSW method

With a view to establishing the spatial resolution of the variable-period XSW technique, zinc position within a series of LB films incorporating zinc alkanolates, which differed in alkyl chain length, was determined. The corresponding  $\langle z \rangle$  data, averaged over the four fluorescence measurements (Table 2) performed on each member of the series, are presented graphically in Fig. 7. The chain length dependence of  $\langle z \rangle$  is apparent from these data, with  $\langle z \rangle$  increasing as chain length increases. The solid line in Fig. 7 shows the calculated  $\langle z \rangle$  dependence on chain length, assuming that all chains in the adlayer are oriented with their

**TABLE 2** Gold surface roughness,  $\sigma_r$ , film thickness,  $d_L$ , zinc mean position,  $\langle z \rangle$ , distribution half-width,  $\sigma$ , lipid adlayer thickness  $d_{m,1}$  and  $d_{m,2}$ , and tilt angle,  $\alpha$ , of zinc alkanates in Langmuir-Blodgett films determined by x-ray reflectivity and fluorescence standing-wave measurements

Sample series*	Chain length	Reflectivity <sup>#</sup>		Fluorescence <sup>#</sup>			$d_{m,1}$ (Å)*	$d_{m,2}$ (Å)*	Tilt angle <sup>§</sup>
		$\sigma_r$ (Å)	$d_L$ (Å)	$\langle z \rangle$ (Å)	$\sigma$ (Å)	$d_L$ (Å)			
A	C18	12.7 ± 0.6	74.8 ± 3.0	41.8 ± 0.6	16.3 ± 0.4	65.6 ± 1.4	19.6 ± 0.8	23.8 ± 1.5	39.7 ± 2.8
	C19	12.9 ± 0.3	74.0 ± 2.0	44.9 ± 0.6	16.2 ± 0.4	70.7 ± 2.6	22.7 ± 0.8	25.8 ± 2.7	32.0 ± 3.2
	C20	12.8 ± 0.6	78.7 ± 3.5	46.1 ± 1.0	16.0 ± 1.0	72.7 ± 2.5	23.9 ± 1.1	26.6 ± 2.7	31.5 ± 4.3
	C21	13.0 ± 0.2	76.6 ± 1.7	47.5 ± 1.2	16.6 ± 0.5	72.1 ± 2.8	25.3 ± 1.3	24.6 ± 3.0	30.3 ± 5.0
	C22	13.5 ± 0.2	80.5 ± 1.5	50.0 ± 0.5	16.5 ± 0.2	76.5 ± 2.5	27.8 ± 0.7	26.5 ± 2.5	24.6 ± 3.1
	C23	12.6 ± 0.6	81.0 ± 1.0	51.0 ± 1.0	16.7 ± 0.4	75.4 ± 3.8	28.8 ± 1.1	24.4 ± 3.9	25.2 ± 4.6
	C24	12.8 ± 1.2	82.5 ± 3.0	55.0 ± 0.7	15.7 ± 0.6	83.8 ± 4.5	32.8 ± 0.9	28.8 ± 4.5	7.8 ± 11.4
B	C20	12.7 ± 0.3	150.7 ± 2.5	47.8 ± 0.2	14.8 ± 0.1	121.0 ± 2.0	25.6 ± 0.5	11.3 ± 2.0	24.0 ± 2.5
C	C21	14.3 ± 0.6	219.8 ± 1.5	171.6 ± 1.2	18.0 ± 1.0	195.3 ± 1.0	25.6 ± 1.3	23.7 ± 5.1	29.1 ± 5.2
	C24	12.8 ± 0.7	228.0 ± 5.0	178.0 ± 1.7	15.8 ± 0.5	204.5 ± 5.0	32.0 ± 2.0	26.5 ± 5.3	14.9 ± 12.1

\*See legend, Fig. 1.

<sup>#</sup>The parameters are reported as the average of values obtained from measurements performed on two distinct parts of duplicate mirrors. The errors were calculated as half of the interval between the minimum and maximum values.

<sup>§</sup>Tilt corresponds to the angle between the long axis of the chains in the first alkanate monolayer and the normal to the mirror substrate surface. The corresponding  $d_{m,1}$ ,  $d_{m,2}$ , and tilt angle uncertainties were calculated by error propagation (Bevington, 1992).

long axis perpendicular to the substrate surface and that the alkyl chains are in the all-*trans* configuration and do not interdigitate. For all but C24, the solid line lies several ångströms above the measured  $\langle z \rangle$  value, suggesting that the chains are tilted for the shorter chain members of the series.

In the case of C24, untilted orientation prevails, as will be discussed.

Each of the  $\langle z \rangle$  data points in Fig. 7 has associated error bars (see Table 2 for description of error calculation). These range from  $\pm 0.5$  Å to  $\pm 1.2$  Å on  $\langle z \rangle$  values of  $\sim 40$ – $55$  Å. Accordingly, we consider the spatial resolving power of the XSW in this type of application to be on the order of 1–2 Å.

The reproducibility of the XSW measurement was evaluated by making XSW measurements of two distinct and nonoverlapping sections of duplicate mirror samples. Averages and associated errors of these four measurements are reported in Table 2 for  $\langle z \rangle$  and  $\sigma$  of the zinc distribution. The latter range from 0.5 Å to 1.2 Å for  $\langle z \rangle$  and from 0.2 Å to 1.0 Å for  $\sigma$ , corresponding to a 1–3% error on  $\langle z \rangle$  and a 6% error on  $\sigma$ . Given the complexity of the sample preparation protocols and the XSW measurements and analysis, reproducibility is quite good.

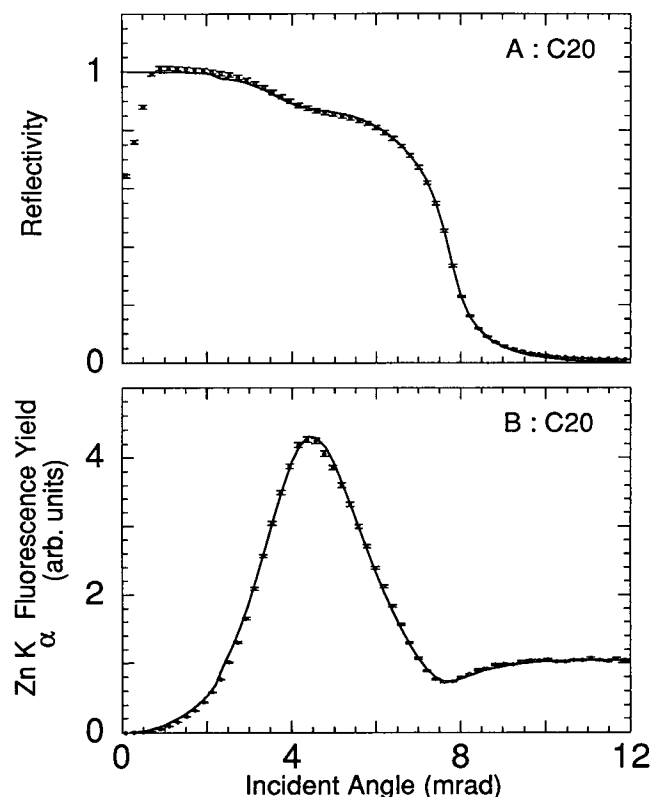


**FIGURE 5** The experimental (circles) and theoretical (solid lines) angular dependence at 9.8 keV of the specular reflectivity (A) and zinc K $\alpha$  fluorescence yield (B) for sample B, consisting of inverted bilayers of zinc arachidate (C20) and  $\omega$ TA on top of a self-assembled ODT monolayer.

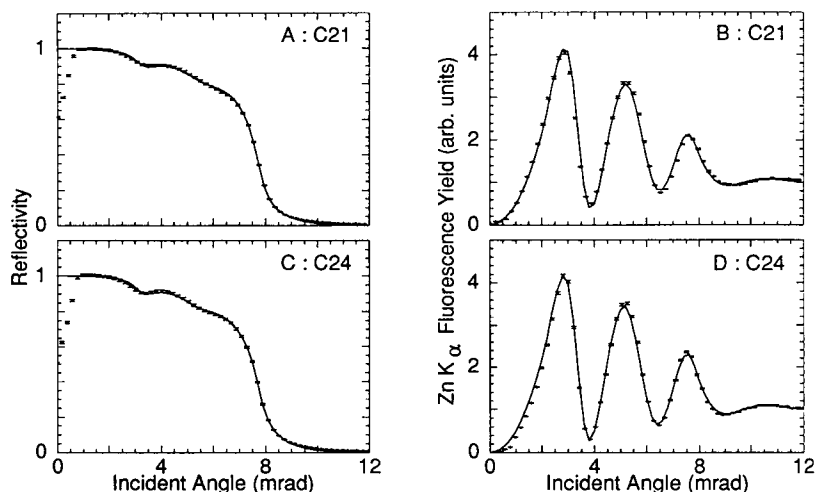
## Zinc label distribution

### Series A (Au/ODT<sub>m</sub>/ZnA<sub>1b</sub>)

As noted above, the zinc mean position,  $\langle z \rangle$ , above the mirror surface increases with alkanate chain length (Table 2 and Fig. 7). However, for  $C \leq 23$ , the measured  $\langle z \rangle$  value is less than expected for a perpendicular orientation, suggesting that the chains in the first alkanate monolayer of thickness  $d_{m,1}$  ( $= \langle z \rangle - d_0$ ; Table 2 and Fig. 1) are tilted in these samples. A tilt angle  $\alpha$  ( $= \cos^{-1} d_{m,1}/L$ ) has been calculated for each of these samples that accounts for the mismatch; these are included in Table 2. To within the uncertainty of the measurements, a similar behavior is observed for the second zinc alkanate monolayer chains (Table 2).

Molecular tilting of the type described above has been observed in the so-called tilted phases of fatty acid salts on aqueous subphase and solid substrate surfaces as deter-

FIGURE 6 The experimental (circles) and theoretical (solid lines) angular dependence at 9.8 keV of the specular reflectivity (A, C) and zinc  $K_{\alpha}$  fluorescence yield (B, D) for series C samples consisting of a self-assembled ODT monolayer overlain by two inverted bilayers of  $\omega$ TA and an inverted bilayer of zinc heneicosanoate (C21) and zinc lignocerate (C24).



mined by x-ray diffraction and reflectivity (Kjaer et al., 1988, 1989; Bohm et al., 1994; Shih et al., 1992; Malik et al., 1995), x-ray absorption (Outka et al., 1987), and atomic force microscopy (Schwartz et al., 1993; Zasadzinski et al., 1994; Viswanathan et al., 1995). Tilting is attributed to a balance of forces acting to optimize van der Waals attractive interactions between alkyl chains and interfacial area of the molecules (Kitaigorodskii, 1961). Theories that emerge from such considerations suggest that the tilt angles must vary with chain length (Safran et al., 1986; Kaganer et al., 1993; Swanson et al., 1996).

The  $\alpha$  angles determined within the observed uncertainties in the current study (Table 2) suggest that for the longest member in this series, C24, the chains are oriented perpendicular to the mirror surface. As chain length decreases, tilt angle increases progressively to a maximum value of  $40^\circ$  in the case of C18. The  $\alpha$  value of  $31.5 \pm 4.3^\circ$  observed for zinc arachidate (C20) in the current study agrees with that determined by AFM for monolayers and multilayers of zinc arachidate deposited directly on hydro-

philic mica and silicon substrates (Zasadzinski et al., 1994; Viswanathan et al., 1995). In these and related AFM studies (Schwartz et al., 1993), it was found that the lattice parameters, symmetry and area per molecule, which in turn determine the tilt angle, are independent of the acyl chain length in the range C16 to C22 for fatty acid salts of  $\text{Cd}^{2+}$ ,  $\text{Mn}^{2+}$ ,  $\text{Ba}^{2+}$ , and  $\text{Pb}^{2+}$ . Although  $\text{Zn}^{2+}$  was not included in the latter chain length study, we find that  $\alpha$  is chain length dependent for zinc alkanates deposited on hydrophobic surfaces extending from C18 to C24 (Table 2).

In terms of zinc atom distribution around its mean position, a  $\sigma$  value of  $16.3 \pm 0.2 \text{ \AA}$  was observed, averaged over the entire homologous series in sample series A.  $\sigma$  is independent of chain length and tilt angle (Table 2). The measured value of  $\sigma$  has at least two contributions. One is from the gold mirror interfacial roughness,  $\sigma_r$  ( $= 12.9 \pm 0.3 \text{ \AA}$ ; Table 2), and the other arises from the intrinsic spread of zinc,  $\sigma_{in}$ , within the LB film. The three quantities are related in the following way:

$$\sigma^2 = \sigma_r^2 + \sigma_{in}^2 \quad (7)$$

It is  $\sigma_{in}$  that we are interested in. Accordingly,  $\sigma_{in}$  is obtained by using Eq. 7, because we have reliable estimates for  $\sigma$  and  $\sigma_r$ . The corresponding value for  $\sigma_{in}$  is  $10.0 \pm 0.5 \text{ \AA}$ , which, as noted above for  $\sigma$ , is independent of chain length in the series A samples.

Parenthetically, we note that recent XSW measurements on LB films composed of zinc and manganese arachidate deposited on a  $280 \text{ \AA}$ -thick gold substrate gave  $\sigma$  and  $\sigma_r$  values of  $7.0 \pm 1.0 \text{ \AA}$  and  $5.6 \pm 0.1 \text{ \AA}$ , respectively, corresponding to a  $\sigma_{in}$  value of  $4.2 \pm 1.7 \text{ \AA}$  (manuscript in preparation). These data suggest that a thinner gold mirror ( $1000 \text{ \AA}$  versus  $280 \text{ \AA}$ ) provides for a smaller  $\sigma_r$  and a correspondingly lower value of  $\sigma_{in}$  for deposited films.

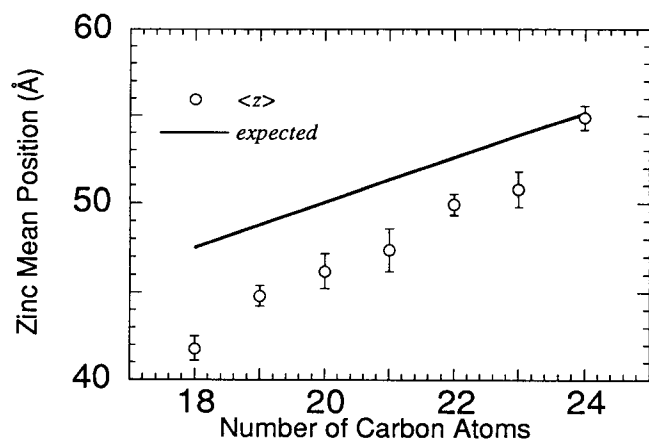


FIGURE 7 Hydrocarbon chain length dependence of zinc mean position ( $z$ ) for sample series A. The solid line represents the corresponding value of the zinc mean position calculated from molecular structure, assuming that all chains are oriented perpendicular to the mirror substrate surface (see text and Fig. 1 for details).

### Sample B (Au/ODT<sub>m</sub>/ZnA<sub>1b</sub>/ωTA<sub>1b</sub>)

Sample B was designed to determine whether the presence of an inverted lipid bilayer ( $\omega$ TA) on top of the zinc arachi-

date (C20) LB film had any effect on the measured zinc distribution parameters  $\langle z \rangle$  and  $\sigma$ . The fluorescence yield data for sample B are consistent with a  $\langle z \rangle$  value of  $47.8 \pm 0.2$  Å. This is to be compared with  $46.1 \pm 1.0$  Å recorded for the corresponding uncoated sample in series A (Table 2). Although the difference is not large, it can be accounted for by a difference in the tilt angle of the arachidate chains in the LB film next to the self-assembled ODT monolayer. The corresponding angles for coated (sample B) and uncoated (series A) samples are  $24.0 \pm 2.5^\circ$  and  $31.5 \pm 4.3^\circ$ , respectively, calculated as described above.

If we assume that the arachidate chains in the second monolayer of the zinc arachidate LB film of sample B are also tilted at an angle of  $24^\circ$ , a total adlayer thickness  $d_L$  ( $= \langle z \rangle + d_{m,1} + d_{\omega TA}$ ) of  $135.3 \pm 0.5$  Å is obtained. The measured value is  $121 \pm 2$  Å (Table 2), based on fluorescence yield data. This result suggests that chain tilt in the second zinc arachidate monolayer is considerably in excess of  $24^\circ$  and/or that tilting prevails in the LB films of  $\omega TA$ .

As far as the distribution of the zinc ions within the alkanolate adlayer is concerned, a  $\sigma$  value of  $14.8 \pm 0.1$  Å was obtained from the fluorescence yield profile fitting which, after deconvoluting the surface roughness,  $\sigma_r = 12.7 \pm 0.3$  Å, leads to a value for the intrinsic distribution half-width,  $\sigma_{in}$ , of  $7.6 \pm 0.5$  Å. This is in contrast to a value of  $10.0 \pm 0.5$  Å obtained for the corresponding uncoated sample in series A (Table 2). Thus the  $\omega TA$  overlayer contributes to a considerable sharpening of the zinc distribution within a coated zinc arachidate LB film. How the overlayer brings about this effect is open to speculation. One possibility is that a direct interaction between the chains of the overlayer and the second zinc arachidate monolayer contributes to a more orderly packing of the latter that propagates down to the polar zinc layer. A similar effect has been observed previously in an x-ray scattering study of alkanolate multilayers on a hydrophobic glass substrate (Skita et al., 1986).

### Series C (Au/ODT<sub>m</sub>/2 $\omega TA_{ib}$ /ZnA<sub>ib</sub>)

With a view to evaluating the influence that a larger distance between the zinc-containing adlayer and the solid substrate has on zinc distribution characteristics, series C samples incorporating two inverted bilayers of  $\omega TA$  sandwiched between the hydrophobic gold surface and an inverted bilayer of zinc heneicosanoate (C21) and zinc lignocerate (C24) were prepared. For C21, an average  $\langle z \rangle$  value of  $171.6 \pm 1.2$  Å (Table 2) was obtained from the fluorescence data, which corresponds to a  $d_{m,1}$  ( $= \langle z \rangle - 2\omega TA_{ib} - d_0$ ) of  $25.6 \pm 1.3$  Å and a tilt angle of  $29.1 \pm 5.2^\circ$ . Within the uncertainty of the measurements, this tilt angle is similar to that observed for the C21 sample in series A ( $30.3 \pm 5.0^\circ$ ; Table 2), which did not include the  $\omega TA$  spacer. If we assume that the first and second monolayers in the LB film are equally tilted, a total film thickness of  $197.2 \pm 1.8$  Å is obtained that agrees with the value ( $195.3 \pm 5.0$  Å) obtained from fluorescence yield profile fitting (Table 2).

For C21 in series C, the zinc distribution characteristic  $\sigma$  is  $18.0 \pm 1.0$  Å (Table 2), which corresponds to a  $\sigma_{in}$  of  $10.9 \pm 1.8$  Å. A similar value ( $10.0 \pm 0.5$  Å) was observed for the C21 sample in series A that lacked the  $\omega TA$  spacer.

The results obtained with zinc lignocerate (C24) parallel those for C21 (Table 2 and Fig. 6), and the conclusions regarding zinc distribution characteristics are the same. Taken together, these data show that  $\omega TA$ , used as a spacer between the inverted bilayer of either zinc heneicosanoate (C21) or zinc lignocerate (C24) and the hydrophobic gold mirror, has no significant effect on the zinc  $\sigma_{in}$  distribution characteristic or the orientation of the hydrocarbon chains within the LB film.

## CONCLUSIONS

The present study demonstrates that the spatial resolution of the variable-period x-ray standing-wave method is on the order of 1–2 Å when applied to LB films with marker atoms positioned some 50 Å above the supporting solid substrate. From repeated measurements on separate LB films, sample preparation, as well as the XSW method itself, is quite reproducible. The intrinsic spread of marker atoms about the mean position within LB films can be determined by deconvoluting mirror surface roughness from the measured marker atom distribution. The data suggest that chain tilt angle in LB films of zinc alkanolates is chain length dependent, decreasing from  $40^\circ$  for C18 to  $0^\circ$  for C24. In contrast, the intrinsic spread about the mean position of the marker atom is not chain length sensitive in the range studied. Shifting the marker layer away from the solid support by 120 Å had little if any effect on the marker atom distribution characteristic  $\sigma_{in}$  or on chain orientation in the zinc alkanolate LB films examined. However, a fatty acid overlayer on top of the zinc alkanolate LB film had a significant ordering effect on marker atom distribution, as reflected in a lower  $\sigma_{in}$ .

The spatial resolution and reproducibility characteristics of the XSW method, in concert with our observations on how film composition influences film structure, suggest that the XSW method will prove itself useful in deciphering the structure of membranes reconstituted with proteins and other molecules. The most immediate challenge is to effect such reconstitution with membranes that are sufficiently uniform and ordered for XSW measurement. Additional requirements for successful implementation of the XSW method as applied to membrane topology have been discussed (Caffrey and Wang, 1995).

Dr. S. Kirchner's participation in the early stages of this project is acknowledged. The authors thank Dr. Jin Wang for helpful discussions and Dr. Paul Lyman for technical support at the X-15A beam line, National Synchrotron Light Source, Brookhaven National Laboratory.

This work was supported by grants from the National Institute of Health (DK 36849 and DK46295) and The Petroleum Research Foundation of the American Chemical Society (30537-AC7) to MC. RI and RZ, respectively, thank Fundação de Amparo à Pesquisa do Estado de São Paulo and

Conselho Nacional de Desenvolvimento Científico e Tecnológico of Brazil and the Graduate School of The Ohio State University for postdoctoral fellowships.

## REFERENCES

- Bedzyk, M. J., G. M. Bommarito, M. Caffrey, and T. L. Penner. 1990. Diffuse-double layer at a membrane-aqueous interface measured with x-ray standing waves. *Science*. 248:52–56.
- Bedzyk, M. J., G. M. Bommarito, and J. S. Schildkraut. 1989. X-ray standing waves at a reflecting mirror surface. *Phys. Rev. Lett.* 62: 1376–1379.
- Bevington, P. R. 1992. *Data Reduction and Error Analysis for the Physical Sciences*. McGraw-Hill, New York.
- Bohm, C., F. Leveiller, D. Jacquemain, H. Míhwald, K. Kjaer, J. Als-Nielsen, I. Weissbuch, and L. Leiserowitz. 1994. Packing characteristics of crystalline monolayers of fatty acid salts, at the air-solution interface, studied by grazing incidence x-ray diffraction. *Langmuir*. 10:830–836.
- Caffrey, M., and J. Wang. 1995. Membrane-structure studies using x-ray standing waves. *Annu. Rev. Biophys. Biomol. Struct.* 24:351–378.
- Carrell, C. J., H. L. Carrell, J. Erlebacher, and J. P. Glusker. 1988. Structural aspects of metal ion-carboxylate interactions. *J. Am. Chem. Soc.* 110:8651–8656.
- de Boer, D. K. G. 1994. Influence of the roughness profile on the specular reflectivity of x-rays and neutrons. *Phys. Rev. B*. 49:5817–5820.
- de Boer, D. K. G. 1995. X-ray reflection and transmission by rough surfaces. *Phys. Rev. B*. 51:5297–5305.
- de Boer, D. K. G. 1996. X-ray scattering and x-ray fluorescence from materials with rough surfaces. *Phys. Rev. B*. 53:6048–6064.
- Gordon, A. J., and R. A. Ford. 1972. *The Chemist's Companion: A Handbook of Practical Data, Techniques and References*. John Wiley & Sons, New York.
- Kaganer, V. M., M. A. Osipov, and I. R. Peterson. 1993. A molecular model for tilting phase transitions between condensed phases of Langmuir monolayers. *J. Chem. Phys.* 98:3512–3527.
- Kirchner, S., J. Wang, Z. Yin, and M. Caffrey. 1995. X-ray standing waves as probes of surface structure: incident beam energy effects. *J. Appl. Phys.* 78:2311–2322.
- Kitaigorodskii, A. I. 1961. *Organic Chemical Crystallography*. Chap. 4. Consultants Bureau, New York. 177–215.
- Kjaer, K., J. Als-Nielsen, C. A. Helm, P. Tippmann-Krayer, and H. Míhwald. 1988. An x-ray scattering study of lipid monolayers at the air-water interface and on solid supports. *Thin Solid Films*. 159:17–28.
- Kjaer, K., J. Als-Nielsen, C. A. Helm, P. Tippmann-Krayer, and H. Míhwald. 1989. Synchrotron x-ray diffraction and reflection studies of arachidic acid monolayers at the air-water interface. *J. Phys. Chem.* 93:3200–3206.
- Malik, A., M. K. Durbin, A. G. Richter, K. G. Huang, and P. Dutta. 1995. Structures of head-group and tail-group monolayers in a Langmuir-Blodgett film. *Phys. Rev. B*. 52:R11654–R11657.
- Outka, D. A., J. Stíhr, J. P. Rabe, J. D. Swalen, and H. H. Rotermund. 1987. Orientation of arachidate chains in Langmuir-Blodgett monolayers on Si(111). *Phys. Rev. Lett.* 59:1321–1324.
- Porter, M. D., T. B. Bright, D. L. Allara, and C. E. D. Chidsey. 1987. Spontaneously organized molecular assemblies. 4. Structural characterization of *n*-alkyl thiol monolayers on gold by optical ellipsometry, infrared spectroscopy, and electrochemistry. *J. Am. Chem. Soc.* 109: 3559–3568.
- Safran, S. A., M. O. Robbins, and S. Garoff. 1986. Tilt and splay of surfactants on surfaces. *Phys. Rev. A*. 33:2186–2189.
- Schwartz, D. K., R. Viswanathan, J. Garnaes, and J. A. Zasadzinski. 1993. Influence of cations, alkane chain length, and substrate on molecular order of Langmuir-Blodgett films. *J. Am. Chem. Soc.* 115:7374–7380.
- Shih, M. C., T. M. Bohanon, J. M. Mikrut, P. Zschack, and P. Dutta. 1992. Pressure and pH dependence of the structure of a fatty acid monolayer with calcium ions in the subphase. *J. Chem. Phys.* 96:1556–1559.
- Sinha, S. K., E. B. Sirota, S. Garoff, and H. B. Stanley. 1988. X-ray and neutron scattering from rough surfaces. *Phys. Rev. B*. 38:2297–2311.
- Skita, V., W. Richardson, M. Filipkowski, A. Garito, and J. K. Blasie. 1986. Overlayer-induced ordering of the disordered surface monolayer in Langmuir-Blodgett multilayer thin films. *J. Physique*. 47:1849–1855.
- Swanson, D. R., R. J. Hardy, and C. J. Eckhardt. 1996. Model calculations of Langmuir monolayers: pressure effects on tilting behavior of idealized amphiphiles. *J. Chem. Phys.* 105:673–677.
- Viswanathan, R., L. L. Madsen, J. A. Zasadzinski, and D. K. Schwartz. 1995. Liquid to hexatic to crystalline order in Langmuir-Blodgett films. *Science*. 269:51–54.
- Wang, J., M. J. Bedzyk, and M. Caffrey. 1992. Resonance-enhanced x-rays in thin films: a structure probe for membranes and surface layers. *Science*. 258:775–778.
- Wang, J., M. J. Bedzyk, T. L. Penner, and M. Caffrey. 1991. Structural studies of membranes and surface layers up to 1000 Å thick using x-ray standing waves. *Nature*. 354:377–380.
- Wang, J., M. Caffrey, M. J. Bedzyk, and T. L. Penner. 1994a. Structure changes in model membranes monitored by variable period x-ray standing waves: effect of Langmuir-Blodgett film thickness on thermal behavior. *J. Phys. Chem.* 98:10957–10968.
- Wang, J., C. J. A. Wallace, I. Clark-Lewis, and M. Caffrey. 1994b. Structure characterization of membrane bound and surface adsorbed protein. *J. Mol. Biol.* 237:1–4.
- Zasadzinski, J. A., R. Viswanathan, L. Madsen, J. Garnaes, and D. K. Schwartz. 1994. Langmuir-Blodgett films. *Science*. 263:1726–1733.